

FIG. 2. Histogram of the effective mass distribution of the two pions from the reaction  $p + p \rightarrow p + p + \pi^+ + \pi^-$ . The solid curve is the phase-space distribution normalized to the same total area.

same spin and parity, and if the  $\zeta$  resonance does not exist, electromagnetic mixing could lead to an order of magnitude higher rate for (a) and (b) than for the usual  $\omega \rightarrow \pi^+ + \pi^- + \pi^0$  (c). On the other hand, Gell-Mann *et al.*<sup>8</sup> calculate the decay mode ratio  $a/c$  to be only  $\sim 5\%$ .

To search for the mode  $\omega \rightarrow \pi^+ + \pi^-$ , we have plotted in Fig. 2 the effective mass  $m^*$  of the  $\pi^+ \pi^-$  combination from 683 events of the type  $p + p \rightarrow p + p + \pi^+ + \pi^-$ . The  $\omega$  decay should appear as a peak at  $\sim 770$  MeV, within the broad band (700-800 MeV) of the  $\rho^0$  decay. Neither the two- $\pi$  decay of the  $\omega$  nor any sign of the expected  $\rho^0 \rightarrow \pi^+ + \pi^-$  is observed. The absence of the  $\rho^0$

can possibly be explained by the fact that it has a cross section comparable to the  $\omega$ , and this small number of events, spread over the broad effective-mass range of the  $\rho^0$ , would not be observed. Considering the strength of the  $\frac{3}{2}, \frac{3}{2} \pi p$  isobar, and the possibility of final state interactions, it is not surprising that multiple-pion resonances appear to have small cross sections when there are two nucleons present.

The authors wish to acknowledge a valuable discussion with J. Bernstein and to thank S. Goudsmit for valuable editorial suggestions.

\*Work performed under the auspices of the U. S. Atomic Energy Commission.

<sup>1</sup>A. Pevsner, P. Kraemer, M. Nussbaum, C. Richardson, P. Schlein, R. Strand, T. Toohig, M. Block, A. Engler, R. Gessaroli, and C. Meltzer, Phys. Rev. Letters **7**, 420 (1961).

<sup>2</sup>B. C. Maglić, L. W. Alvarez, A. H. Rosenfeld, and M. L. Stevenson, Phys. Rev. Letters **7**, 178 (1961); N. H. Xuong and G. R. Lynch, Phys. Rev. Letters **7**, 327 (1961).

<sup>3</sup>E. L. Hart, R. I. Louttit, D. Luers, T. W. Morris, W. J. Willis, and S. S. Yamamoto, Phys. Rev. **126**, 747 (1962).

<sup>4</sup>P. L. Bastien, J. P. Berge, O. I. Dahl, M. Ferro-Luzzi, D. H. Miller, J. J. Murray, A. H. Rosenfeld, and M. B. Watson, Phys. Rev. Letters **8**, 114 (1962).

<sup>5</sup>E. Pickup, D. K. Robinson, and E. O. Salant, Phys. Rev. Letters **8**, 329 (1962).

<sup>6</sup>Y. Nambu and J. J. Sakurai, Phys. Rev. Letters **8**, 79 (1962).

<sup>7</sup>G. Feinberg, Phys. Rev. Letters **8**, 151 (1962).

<sup>8</sup>M. Gell-Mann, D. Sharp, and W. G. Wagner, Phys. Rev. Letters **8**, 261 (1962).

### $K^+ - p$ INTERACTION FROM 140 TO 642 MeV/c\*

Sulamith Goldhaber, William Chinowsky, Gerson Goldhaber,  
Wonyong Lee, Thomas O'Halloran, and Theodore F. Stubbs  
Lawrence Radiation Laboratory, University of California, Berkeley, California

and

G. M. Pjerrou, Donald H. Stork, and Harold K. Ticho  
Department of Physics, University of California, Los Angeles, California  
(Received July 2, 1962)

A detailed investigation of the energy dependence of the  $K^+$ -proton scattering cross section at low momenta has been carried out. In the region from 140 to 642 MeV/c, the nuclear cross section varies little with energy. The cross sections are distinctly lower than values quoted earlier.<sup>1</sup> The momentum dependence of the phase shifts below 300 MeV/c can only be interpreted as  $s$ -wave scattering and

does not admit isotropic  $p$ -wave solutions such as were obtained as possible ambiguities at 810 MeV/c.<sup>2</sup> The isotropy in the differential cross sections and the constructive interference with Coulomb scattering at each of the momenta show that the repulsive  $s$ -wave character of the  $K^+ - p$   $T=1$  state persists throughout this region.

An  $s$ -wave effective-range fit to the experimental

$K^+ - p$  data up to 642 MeV/c gives, for the scattering length,  $a = -0.29 \pm 0.015$  fermi and, for the effective range,  $r_0 = 0.5 \pm 0.15$  F. It should be noted that for the highest momentum included in the fit, the quantities  $|ak|$  and  $r_0 k$  remain below unity. Alternatively, the data can also be represented by a purely repulsive core of radius  $r_c = 0.31 \pm 0.01$  F.

The experimental data for this analysis were obtained from photographs taken with the 15-inch LRL bubble chamber. A mass-separated  $K^+$  beam described earlier<sup>2</sup> was conveyed by a beam transport system at 645 MeV/c. The background of light particles (pions, muons, and electrons) was approximately 0.5%. The method of analysis of the data at 642 MeV/c is very similar to that described earlier.<sup>2</sup> At this momentum only about 0.5% of the total cross section, or about  $0.06 \pm 0.03$  mb, is due to inelastic pion production.<sup>3</sup>

Four distinct series of pictures taken are described here, the first with the direct  $K^+$  beam giving  $642 \pm 7$  MeV/c in the chamber and three more with various thicknesses of tungsten absorbers placed immediately ahead of the chamber. This gave average momenta of  $520 \pm 15$ ,  $355 \pm 25$ , and approximately 220 MeV/c, respectively. At the lowest-momentum series the initial spread of the beam, as well as the energy loss in the absorber and in the chamber liquid, yields a  $K$ -meson path-length distribution over the momentum interval from zero to 300 MeV/c. Since the path length falls off rapidly at the edges of the momentum distribution, we have accepted for the purpose of cross-section determinations a momentum band from 120 to 280 MeV/c, which we divided into five momentum intervals.

The momenta of all  $K$ -H interactions were determined by kinematical fitting at the interaction point. The path lengths contributing to the various momentum intervals were computed from the number of "tau" decays in flight, their known mean life, and the  $K^+$  branching ratio into this decay mode. For this purpose all three-prong "tau-like" decays were measured. From kinematical fitting it was possible (a) to select the true  $\tau$ -meson mode, and (b) to get an accurate momentum at which the  $\tau$  decay occurred.<sup>4</sup> At the lowest momentum band (120 to 280 MeV/c), where the path-length distribution was particularly critical, we measured 10% of all tracks and obtained the path-length distribution from the measured momentum distribution and the measured track lengths. This provided an additional method independent of the  $\tau$ -decay distribution.

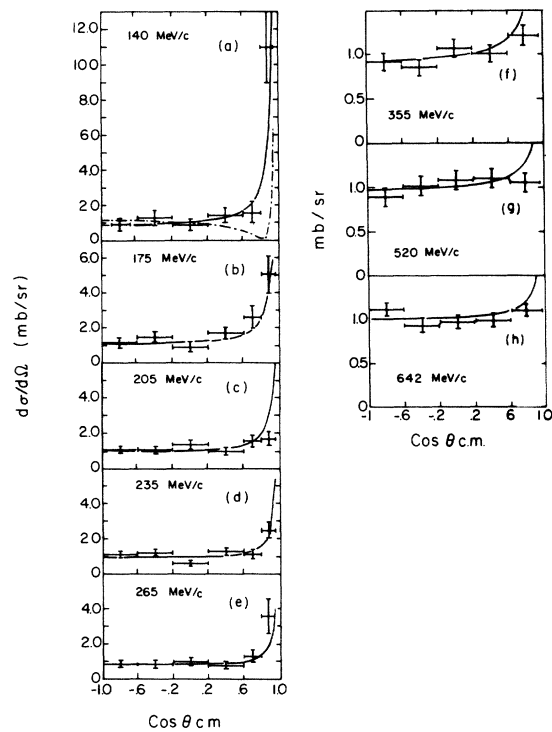


FIG. 1. The differential  $K^+ - p$  cross section at the various momenta. The solid curves correspond to the differential cross sections computed for repulsive  $s$ -wave scattering. The corresponding phase shifts are given in Table I. The dashed curve in Fig. 1(a) illustrates the effect of an attractive  $s$ -wave phase shift fitted up to  $\cos \theta_{c.m.} = 0.6$ .

The experimental differential cross sections are shown in Fig. 1. We have taken a cutoff at a scattering angle corresponding to  $\cos \theta_{c.m.} = 0.95$ , beyond which detection efficiencies decrease rapidly. The repulsive  $K^+ - N$  potential is evident at all momenta, and, in particular, in the lowest momentum interval, where the constructive interference with Coulomb scattering is most striking.

The isotropic character of the  $K^+ - p$  differential cross section can be fitted for any single momentum interval by (a) pure  $s$ -wave scattering, (b)  $p_{1/2}$ -wave scattering, and (c) a suitable mixture of  $p_{1/2}$ - and  $p_{3/2}$ -wave scattering. These ambiguities were discussed in detail in our earlier work at 810 MeV/c.<sup>2</sup> However, with the series of momenta we have available now, it becomes clear that the  $p$ -wave solutions can be ruled out. In particular at momenta below 300 MeV/c the phase-shift behavior disagrees clearly with  $p$  waves, i.e.,  $\tan \delta \propto k^3$ . Furthermore, the varia-

tion of  $\delta$  with momentum is smooth up to 810 MeV/c; hence a switchover to one of the  $p$ -wave solutions appears extremely unlikely.

The differential cross sections were computed by using pure  $s$ -wave and Coulomb scattering amplitudes:

$$\frac{d\sigma}{d\Omega} = \frac{1}{k^2} \left| e^{i\delta_1} \sin \delta_1 - \frac{\alpha}{2 \sin^2(\theta/2)} \exp \left[ -i\alpha \ln \sin^2 \left( \frac{\theta}{2} \right) \right] \right|^2, \quad (1)$$

where

$$\alpha = e^2 / \hbar v_{\text{rel}},$$

$\hbar k$  = the center-of-mass momentum,  $v_{\text{rel}}$  = the relative velocity, and  $\delta_1$  = the  $s$ -wave phase shift. The continuous curves shown in Fig. 1,  $a$  through  $h$ , are based on the repulsive  $s$ -wave phase shifts.

Table I lists these phase shifts as well as the experimental data from which they were computed. Column 2 gives the total cross section<sup>5</sup> up to  $\cos \theta_{\text{c.m.}} = 0.85$ . The phase shifts, column 4, were computed by equating the experimental cross sections with the corresponding integral over Eq. (1). The total nuclear cross sections given in column 3 have been computed from  $\sigma = 4\pi \sin^2 \delta_1 / k^2$ . The above procedure actually yields two  $s$ -wave phase shifts, an attractive and a repulsive one. For illustration the dashed curve in Fig. 1 shows the

Table I.  $K^+p$  cross sections and phase shifts from 140 to 642 MeV/c. The experimental cross sections are quoted up to a cutoff angle corresponding to  $\cos \theta_{\text{c.m.}} = 0.85$ . The nuclear cross sections are computed up to  $\cos \theta_{\text{c.m.}} = 1$ , for pure repulsive  $s$ -wave scattering. The last column gives the corresponding phase shifts.

$P_K$ (MeV/c)	Experimental	$T = 1$ S-wave fit	
	$\sigma$ nuclear + Coulomb for $\cos \theta_{\text{c.m.}} \leq 0.85$ (mb)	$\sigma$ nuclear (mb)	$\delta_1$ (deg)
140 ± 20	14.9 ± 2.5	9.2 ± 2.1	-7.2 ± 0.8
175 ± 15	16.0 ± 2.4	12.5 ± 2.2	-10.4 ± 0.9
205 ± 15	13.7 ± 1.8	11.5 ± 1.7	-11.7 ± 0.9
235 ± 15	12.7 ± 1.6	11.2 ± 1.6	-13.2 ± 0.9
265 ± 15	11.0 ± 1.6	10.0 ± 1.6	-14.0 ± 1.1
355 ± 25	11.9 ± 1.2	11.7 ± 1.2	-20.0 ± 1.1
520 ± 15	11.9 ± 1.2	12.2 ± 1.3	-29.4 ± 1.7
642 ± 7	11.9 ± 0.8	12.4 ± 0.9	-36.2 ± 1.4

differential cross section for the attractive solution  $\delta_1 = +10.5^\circ$  fitted up to  $\cos \theta_{\text{c.m.}} = 0.6$ . It is clear by comparison with the experimental differential cross sections that the attractive solutions can be eliminated. Figure 2 illustrates the behavior of the experimental total cross sections, the total nuclear cross sections, and the repulsive  $s$ -wave phase shifts as a function of the momentum in the laboratory system.

We have further shown that the data up to 642 MeV/c can be well represented with a two-parameter effective-range approximation. A least-squares fit to the integrated cross sections<sup>6</sup> up to 355 MeV/c with the constraint of  $k \cot \delta = (1/a) + \frac{1}{2} r_0 k^2$  allows the determination of the scattering length to within less than 10% ( $a = -0.29 \pm 0.02$  F), but leaves large uncertainties in the effective range<sup>7</sup> ( $r_0 = 0.6 \pm 0.6$  F). In this momentum inter-

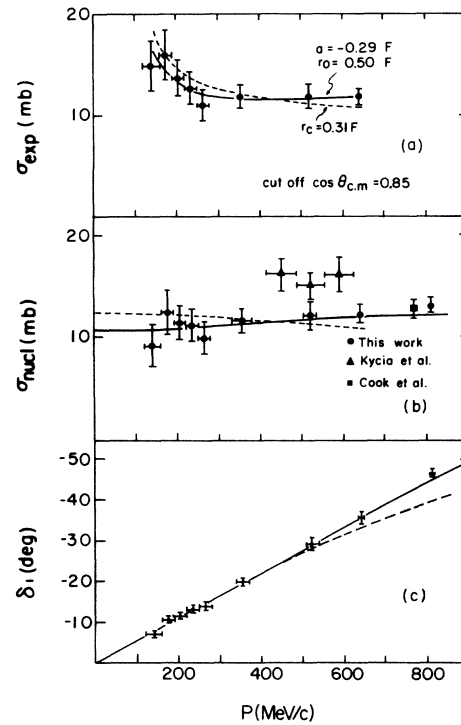


FIG. 2. (a) Variation of the measured cross section with laboratory momentum up to a cutoff angle taken at  $\cos \theta_{\text{c.m.}} = 0.85$ . (b) Corresponding total nucleon cross sections, computed with a repulsive phase shift. Also given for comparison are the data of Kycia *et al.* (reference 1) and Cook *et al.*,<sup>9</sup> as well as our own data at 810 MeV/c (reference 2). (c) Repulsive  $s$ -wave phase shifts. It should be noted that at 810 MeV/c about 1 mb of inelastic scattering is included (reference 2). The solid curves correspond to the effective-range fit up to 642 MeV/c, the dashed curves to the fit with a purely repulsive core.

Table II. Summary of the effective-range approximation and potential fit to the experimental  $K^+p$  scattering cross section.

Momentum interval (MeV/c)	$a$ ( $10^{-13}$ cm)	$r_0$ ( $10^{-13}$ cm)	$r_c$ ( $10^{-13}$ cm)	Probability from a $\chi^2$ fit
Effective-range approximation				
140-355	$-0.29 \pm 0.02$	$0.6 \pm 0.6$		75 %
140-642	$-0.29 \pm 0.015$	$0.5 \pm 0.15$		85 %
Zero-range approximation				
140-355	$-0.3 \pm 0.01$	0		65 %
140-642	$-0.33 \pm 0.01$	0		1 %
Hard core				
140-642			$0.31 \pm 0.01$	40 %

val the quantities  $|ak|$  and  $r_0k$ , which test the validity of the effective-range expansion, remain well below unity. It is remarkable, however, that the values of the parameters hardly change when we include data up to 642 MeV/c in the least-squares fit. The values for the scattering length and effective range now become  $a = -0.29 \pm 0.015$  F and  $r_0 = 0.5 \pm 0.15$  F, respectively,<sup>8</sup> with a goodness of fit ( $\chi^2$ ) corresponding to an 85% probability. It should be noted here that upon inclusion of the higher momenta the uncertainty in  $r_0$  has been decreased appreciably.

Finally we have also attempted to fit the experimental data directly to a phenomenological potential. The potential considered was a repulsive hard core of radius  $r_c$  followed by an attractive well of range  $r_a$  and depth  $V$ .

We find that the experimental data lack the statistical accuracy needed to determine the three parameters. It should be noted, however, that a one-parameter fit, setting  $V = r_a = 0$ , fits the data up to 642 MeV/c with a 40% probability, giving a hard-core radius  $r_c = 0.31 \pm 0.01$  F. These results, as well as the consequences from insisting on a zero-range approximation, are given in Table II.

\*Work done under the auspices of the U. S. Atomic Energy Commission.

<sup>1</sup>T. F. Kycia, L. T. Kerth, and R. G. Baender, Phys. Rev. **118**, 553 (1960).

<sup>2</sup>T. F. Stubbs, H. Bradner, W. Chinowsky, G. Goldhaber, S. Goldhaber, W. Slater, D. H. Stork, and H. K. Ticho, Phys. Rev. Letters **7**, 188 (1961).

<sup>3</sup>G. Fisk, D. H. Stork, H. K. Ticho, W. Chinowsky, G. Goldhaber, S. Goldhaber, and T. F. Stubbs (to be published).

<sup>4</sup>We were able to utilize this method down to the lowest momentum considered here. Even at  $P_K \approx 120$  MeV/c, the separation between a  $\tau$  decay "at rest" and "in flight" was quite definite.

<sup>5</sup>This smaller angle was chosen so as to avoid regions of poorer scanning efficiency. Corrections have been made to the data for scanning bias in the distribution of the azimuthal angle  $\phi$ . The corrections become very small if we stay away from the angles for which  $\cos\theta_{c.m.} > 0.85$ .

<sup>6</sup>We have shown that the least-squares fits are not sensitive to the cutoff angle by varying the latter as well as dividing the data into two angular intervals in the fitting procedure.

<sup>7</sup>Here it should be remarked that the two parameters are actually strongly correlated and the errors quoted are the diagonal elements of error matrix only. The error matrix is  $\begin{pmatrix} 0.00042 & 0.011 \\ 0.011 & 0.344 \end{pmatrix}$ .

<sup>8</sup>The error matrix is now  $\begin{pmatrix} 0.00014 & 0.0012 \\ 0.0012 & 0.015 \end{pmatrix}$ .

<sup>9</sup>V. Cook, D. Keefe, L. T. Kerth, P. G. Murphy, W. A. Wenzel, and T. F. Zipf, Phys. Rev. Letters **7**, 182 (1961).